A 1-DOF Assistive Exoskeleton with Inertia Compensation: Effects on the Agility of Leg Swing Motion

Gabriel Aguirre-Ollinger and J. Edward Colgate and Michael A. Peshkin

Department of Mechanical Engineering, Northwestern University, Evanston, IL 60208, USA

Ambarish Goswami

Honda Research Institute, Mountain View, CA 94041, USA

Abstract

Many of the current implementations of exoskeletons for the lower extremities are conceived to either augment the user's load-carrying capabilities or reduce muscle activation during walking. Comparatively little research has been conducted on enabling an exoskeleton to increase the agility of lower-limb movements. One obstacle in this regard is the inertia of the exoskeleton's mechanism, which tends to reduce the natural frequency of the human limbs.

A control method is presented that produces an approximate compensation of the inertia of an exoskeleton's mechanism. The controller was tested on a statically mounted, single-DOF exoskeleton that assists knee flexion and extension. Test subjects performed multiple series of leg-swing movements in the context of a computer-based, sprint-like task. A large initial acceleration of the leg was needed for the subjects to track a virtual target on a computer screen. The uncompensated inertia of the exoskeleton mechanism slowed down the transient response of the subjects' limb, in comparison with trials performed without the exoskeleton. The subsequent use of emulated inertia compensation on the exoskeleton allowed the subjects to improve their transient response for the same task.

Keywords:

Exoskeleton, rehabilitation robotics, lower-limb assistance, admittance control

1 Introduction

In recent years, different types of exoskeletons and orthotic devices have been developed to assist lower-limb motion. An exoskeleton can be defined as a powered wearable mechanism with an

anthropomorphic configuration, capable of tracking the user's movements. Most of the existing implementations of lower-limb exoskeletons can be classified in the following categories:

- Gravitational support of a load carried by the user.
- Augmentation of the user's muscle forces.
- Gait trainers for physical therapy and movement rehabilitation.
- Single-joint orthotic devices.

An example in the first category is the Berkeley Lower Extremity Exoskeleton (BLEEX) [1], an energetically autonomous exoskeleton designed to support a heavy backpack carried by the user. The device's sensitivity to the user's movements is increased by a controller that employs positive kinematic feedback. The exoskeleton developed by Walsh et al. [2] combines passive load-carrying capabilities with the use of elastic components to store energy during the negative-work phases of the gait cycle. This energy is released during the positive-work phases to assist the progression of walking.

Force augmentation is exemplified by the Hybrid Assistive Leg (HAL) [3], which employs actuators to assist the hip and knee joints. The system utilizes a hybrid control method that combines impedance control for user comfort [4] with an assistive mode of operation, for example EMG-based force augmentation [5].

Robotic gait trainers are usually statically-supported devices designed to assist subjects walking on a treadmill rather than enable autonomous ambulation. Control methods for such devices focus on the mode of transmitting forces to the leg segments. The Lokomat orthosis (Hocoma AG, Volketswil, Switzerland) [6] is designed for automated treadmill training for patients with severe impairment of the lower limbs. Banala et al. [7] have developed a force-controlled active exoskeleton that generates a prescribed trajectory path for the ankle during walking. The Lower-Extremity Powered Exoskeleton (LOPES) [8], has joints actuated with bowden-cable driven series elastic actuators, making the orthosis behave as a force source that acts in substitution of a human trainer.

Active orthoses that assist a single leg joint are usually simpler from an engineering perspective, but often incorporate more expertise on the dynamics and energetics of human walking. Ferris [9] developed a powered ankle–foot orthosis (AFO) that uses proportional electromyographical (EMG) control. The AFO is remarkable in that it has been able to reduce net

metabolic power during walking [10]. The MIT Ankle–Foot Orthosis [11] is a powered AFO designed to assist drop-foot gait. The RoboKnee [12] is a knee-mounted exoskeleton that adds power to the knee joint by means of a linear series elastic actuator.

Significant advances have been made in endowing exoskeletons with force-augmentation capabilities. However, recent surveys [13, 14] reveal that little research has been done so far on the effects of an exoskeleton on the the agility of leg movements. At this point the authors are not aware of any studies specifically addressing how an exoskeleton can influence the subject's self-selected speed of walking. Another topic that has yet to be investigated is the effect of an exoskeleton on the user's ability to accelerate the legs when quick reactions are needed.

The present study constitutes a first step towards enabling an exoskeleton to increase the agility of the lower extremities. At preferred walking speeds, the swing leg behaves as a pendulum oscillating close to its natural frequency [15]. The swing phase of walking takes advantage of this pendular motion of the leg in order to reduce the metabolic cost of walking. Thus a basic notion motivating this research is that a wearable exoskeleton could be used to increase the natural frequency of the legs, an in doing so enable users to walk comfortably at higher speeds. Although a few studies have been conducted on the modulation of leg swing frequency by means of an exoskeleton [16, 4], this effect has not yet been linked to the kinematics and energetics of walking.

A key difficulty in using an exoskeleton to increase the agility of leg movements is that the exoskeleton's mechanism adds weight and inertia to the leg, plus friction and other dissipative effects. Therefore the mechanism by itself will probably tend to make the legs' movements slower, not faster. And while it is quite feasible to mask the weight and the friction of the exoskeleton using control, compensating the mechanism's inertia is considerably more difficult due to stability issues [17, 18]. All other things being equal, the inertia added by the exoskeleton will reduce the pendulum frequency of the legs.This can have important consequences on the kinematics and energetics of walking. A study by Browning [19] found that adding masses to the leg increases the metabolic cost of walking. This cost was strongly correlated to the moment of inertia of the loaded leg. A similar study by Royer [20] showed that loading the legs also increases the swing time and the stride time during walking, which is consistent with a decrease in the natural frequency of the legs.

Although the inertia of the exoskeleton could be kept relatively low through design (for example by using lightweight materials or placing the actuators proximally to the trunk), it

is highly desirable to have a method for compensating the inertia of the exoskeleton through control. This in turn leads to an interesting prospect: to not only compensate the drop in the natural frequency of the legs caused by the exoskeleton mechanism, but to actually make the natural frequency of the exoskeleton-assisted leg *higher* than that of the unaided legs. By thus raising the bandwidth of the leg's frequency response, the exoskeleton may enable users to impart larger accelerations on the legs. Melzer [21] has reported that the velocity of voluntary and compensatory stepping decreases considerably with age. In this regard, an exoskeleton cannot help the age-related deterioration of neurological factors. However, inertia compensation could partially compensate the slowing down of the response of the nervous system by improving the frequency response of the lower limbs.

In this paper a control method is presented that produces an approximate form of compensation of an exoskeleton's inertia. The implementation discussed here is restricted to single-joint control, but it can in principle be transferred to multijoint exoskeleton control. The method was tested on a statically mounted, single-DOF exoskeleton [22, 23] that assists the user in performing knee flexions and extensions. Experiments were conducted in which subjects performed multiple series of leg-swing movements in the context of a computer-based pursuit task. The experimental conditions included moving the leg unaided, and then doing so with the aid of the exoskeleton. The main goal was to determine how the subjects' ability to accelerate their legs was affected by the inertia of the exoskeleton, and to assess the effectiveness of the controller in counteracting these inertial effects.

2 Methods

2.1 Design and control of a 1-DOF exoskeleton with emulated inertia compensation

The authors have designed and built a stationary 1-DOF exoskeleton for assisting knee flexion and extension exercises. Its purpose is to investigate the effects of the exoskeleton's virtual dynamics (i.e. the dynamics resulting from closed-loop control) on the kinematics of leg-swing motion. Figure 1 shows the exoskeleton's main assembly, consisting of a servo motor, a cable-drive transmission and a pivoting arm. The cable-drive solution avoids the occurrence of backlash in the transmission, thereby eliminating the risk of limit cycles during the exoskeleton's operation.

The motor is a Kollmorgen (Radford, VA, USA) brushless AC servo with a power rating of 0.99 kW and a continuous torque rating of 2.0 N-m. The transmission ratio of the cable drive is 10:1, thus allowing a continuous torque output of about 20.0 N-m. The motor comes with a proprietary 24-bit "smart feedback" device that produces an emulated encoder output of up to 32,768 counts before quadrature, for a net resolution of 131,072 counts. The angular position of the exoskeleton arm is obtained from the emulated encoder output. The angular acceleration of the exoskeleton arm is measured by means of an MT9 digital inertial measurement unit from Xsens Technologies (Enschede, the Netherlands), operating at a sampling rate of 200 Hz. The unit features a 3-axis linear accelerometer, and is mounted on the exoskeleton arm in such a way that two of the accelerometer axes lie on the plane of rotation of the arm. Angular acceleration is computed from the linear acceleration readings generated by those two axes[1]. For actual use the exoskeleton assembly is mounted on a rigid support frame (Figure 2). A custom-built, sliding ankle brace couples the user's leg to the exoskeleton arm. Further details of the exoskeleton's design can be found in [24].

Admittance control is employed to make the exoskeleton display a set of chosen virtual dynamics. Experiments using negative virtual damping to transmit energy to the human limb have been reported by the authors [22, 23]. That method relied in part on the passive damping of the human limb to insure the stability of the coupled system formed by the limb and the exoskeleton. However, the same strategy cannot be applied to produce inertia compensation; it is not feasible to implement a negative inertia on the admittance controller and use the inertia of the human limb to guarantee stability. Non-collocation of the exoskeleton's actuator and the torque sensor will cause the coupled system to become unstable even for *positive* values of virtual inertia, if these are too low in magnitude.

The relationship between non-collocation and the exoskeleton's virtual inertia (as generated by the admittance controller) has been analyzed previously [25]. A simple admittance control model showed that the system would become unstable if the virtual inertia was lower than the servo motor's inertia reflected on the shaft of the exoskeleton's arm. The alternative proposed was an approximate form of inertia compensation that used feedback of the low-pass filtered angular acceleration of the exoskeleton arm. A negative feedback gain was employed to approximate the effect of a negative inertia term at low frequencies. Although this technique does not

[1]This method produces a relatively noise-free acceleration signal that would be practically impossible to duplicate by taking a double time derivative of the encoder readings.

attain an exact cancelation of the human limb's inertia, the method does produce some of its desirable effects, particularly an increase in the pendulum frequency of the leg. Thus the effect can be referred to as *emulated inertia compensation*.

2.2 Implementation of the admittance controller with inertia compensator

2.2.1 Structure of the admittance controller

The controller implemented for the physical 1-DOF exoskeleton is shown in Figure 3. Its major components are an admittance controller and a feedback loop forming the inertia compensator. The admittance controller consists of an admittance model followed by a trajectory-tracking LQ controller with an error-integral term [26]. The admittance model is expressed in state-space form as

$$\begin{bmatrix} \dot{\theta} \\ \ddot{\theta} \\ \dot{\xi} \end{bmatrix} = \begin{bmatrix} 0 & 1 & 0 \\ -\frac{\bar{k}_e^d}{I_e^d} & -\frac{\bar{b}_e^d}{I_e^d} & 0 \\ 1 & 0 & 0 \end{bmatrix} \begin{bmatrix} \theta \\ \dot{\theta} \\ \xi \end{bmatrix} + \begin{bmatrix} 0 \\ \frac{1}{I_e^d} \\ 0 \end{bmatrix} \tau_{net} \tag{1}$$

where θ is the angular position of the exoskeleton arm and $\xi = \int \theta dt$. The integral term ξ is employed to minimize tracking error. The input to the admittance model, τ_{net}, is the sum of the torque measured by the torque sensor, τ_s, plus the feedback torque from the inertia compensator. The above system can be expressed in compact form as

$$\dot{\mathbf{q}} = \bar{\mathbf{F}}_\mathbf{e}^\mathbf{d}\mathbf{q} + \bar{\mathbf{G}}_\mathbf{e}^\mathbf{d}\tau_{net} \tag{2}$$

where $\mathbf{q}$ represents the state-space vector

$$\mathbf{q} = [\ \theta \quad \dot{\theta} \quad \xi\ ]^T \tag{3}$$

The admittance model uses numerical integration to generate the reference state-space trajectory $\mathbf{q}_{ref}(t)$ that will be tracked by the closed-loop LQ controller. The reference angle $\theta(t)$ and angular velocity $\dot{\theta}(t)$ are computed using a fourth-order multistep predictor-corrector algorithm. The algorithm was selected for its capability to simulate a physical system with unstable components [27], as is the case of the exoskeleton. Given a sampling period T, the k-th order predictor step is an Adams-Bashforth formula [28], essentially an extrapolation of values computed at times t, $t - T$, etc.:

$$P(\theta) : \theta(t+T) = \theta(t) + T\dot{\theta}(t) + T^2 \sum_{i=1}^{k-1} \alpha_I f(t + [1-i]T) \tag{4}$$

$$P(\dot{\theta}) : T\dot{\theta}(t+T) = \theta(t+T) - \theta(t) + T^2 \sum_{i=1}^{k-1} \alpha'_I f(t + [1-i]T) \tag{5}$$

The next step is an evaluation of f using the predictions $\theta(t+T)$ and $\dot{\theta}(t+T)$. Corrections are then made with the aid of an Adams-Moulton formula:

$$C(\theta) : \theta(t+T) = \theta(t) + T\dot{\theta}(t) + T^2 \sum_{i=1}^{k-1} \beta_i f(t + [2-i]T) \tag{6}$$

$$C(\dot{\theta}) : T\dot{\theta}(t+T) = \theta(t+T) - \theta(t) + T^2 \sum_{i=1}^{k-1} \beta'_i f(t + [2-i]T) \tag{7}$$

The integral term $\xi(t)$ is computed using a simple trapezoidal integral. Kinematic feedback consists of the exoskeleton's arm angle θ, measured by the emulated encoder. A state observer with a Kalman filter $\mathbf{C}(s)$ is provided to compute an estimate of the full feedback state. The controller was implemented in the QNX real-time operating system, using a sampling rate of 1 kHz.

The frequency response of the exoskeleton mechanism showed that the second-order LTI model was sufficiently accurate for frequencies up to 10 Hz [24]. The trajectory-tracking fidelity was estimated with the coefficient of determination, R^2. For a 2 Hz sinusoid the tracking fidelity was found to be 99.3%. Thus the admittance controller can accurately track angular trajectories in the typical frequency range of lower-limb motions.

2.2.2 Implementation of emulated inertia compensation

The estimated angular acceleration is low-pass filtered by means of a fourth-order Butterworth filter. In order to produce the inertia compensation effect, a negative feedback gain I_c is applied. This gain can be considered as a negative inertia term at low frequencies. The cutoff frequency of the low-pass filter is 4 Hz. At higher cutoff frequencies, the frequency content in the acceleration feedback makes it harder to control voluntary leg movements. This frequency content is due in great part to compliance in the coupling between the human limb and the exoskeleton. Very low values of cutoff frequency, on the other hand, reduce the fidelity of the inertia compensation effect due to phase lag. Thus the selected cutoff frequency represents a design compromise in

terms of frequency content and phase lag[2].

In the absence of inertia compensation ($I_c = 0$), the controller makes the exoskeleton behave as a pure inertia. In other words, the controller masks the exoskeleton arm's weight and damping from the user. This is accomplished by making the coefficients of virtual damping $\bar{b}_e^d$ and virtual stiffness $\bar{k}_e^d$ cancel, respectively, with the physical damping b_{arm} and the gravitational "spring constant" k_{arm} of the exoskeleton's arm. Given the location of the torque sensor (port S in Figure 3), the inertia felt by the user when $I_c = 0$ is the sum of the physical inertia of the exoskeleton's arm, I_{arm} (0.185 kg-m^2), plus the baseline virtual inertia generated by the admittance controller, $\bar{I}_e^d$ (set to 0.035 kg-m^2 in the experiments presented here). So in theory the emulated inertia compensator has to counteract a total inertia $\bar{I}_e^d + I_{arm}$ (0.22 kg-m^2) before it can compensate the inertia of the leg itself.

2.2.3 Exoskeleton impedance at the port of interaction with the user

Figure 3 shows parametric plots of the exoskeleton's complex impedance at the port of interaction P for different inertia compensation gains I_c and leg swing frequencies f_c. An analysis of these plots reveals that emulated inertia compensation actually produces a double assistive effect. It not only increases the natural frequency of the coupled system formed by the human limb and the exoskeleton, but also makes the exoskeleton perform net positive work on the limb per swing cycle. This net work is due to the fact that the exoskeleton's impedance at the interaction port has a negative real part. Figure 4 shows parametric plots of the exoskeleton's complex impedance $Z_e^p(j\omega_c)$ at port P for different swing frequencies f_c (with $\omega_c = 2\pi f_c$) and different inertia compensation gains I_c. It can be seen that for I_c <0 the real part of $Z_e^p(j\omega_c)$ is negative as well. Therefore $Re\{Z_e^p(j\omega_c)\}$ can be thought of as a negative damping term that varies with ω_c. This term causes the exoskeleton to transfer net energy to the human leg, rather than draw energy form it as an actual damper would.

2.3 Experiment design

2.3.1 Experimental task

An experiment was conducted to determine the effect of emulated inertia compensation on a subject's ability to perform movements requiring high accelerations. The experimental task was

[2]Because of the low cutoff frequency of the filter, the frequency resolution of the acceleration signals was not an issue in spite of the relatively low sampling rate (200 Hz).

presented to the subject by means of a computer graphic interface, shown in Figure 5. The display showed two cursors traversing the display from left to right. The "target" cursor had a constant linear speed. The other cursor moved in response to the swing motion of the subject's leg; its linear speed was directly proportional to the RMS angular velocity of leg swing, Ω_h. The instruction to the subject was to make his cursor track the position of the target. Because the target cursor moved at a constant speed from the beginning of the trial, a large initial acceleration of the leg was necessary to make the subject's cursor catch up with the target. The experiment consisted of three series of tracking trials. Each series was performed under one of the following experimental conditions:

- UNCOUPLED. Subjects swung the leg unaided. The MT9 inertial measurement unit was attached to the ankle in order to measure the angular velocity and angular acceleration of the subject's limb. (Angular velocity data is produced by the turn-rate gyroscope in the inertial unit.)

- BASELINE. Subjects swung the leg using the exoskeleton with zero inertia compensation; thus the leg was subject to the full inertia of the exoskeleton's arm. The weight of the exoskeleton's arm and the friction and damping of the exoskeleton's drive were canceled by the admittance controller.

- ASSIST. Subjects used the exoskeleton with a specific level of inertia compensation, given by the gain I_c.

The standard duration of each trial was 15 s. For all experimental conditions, the velocity of the target cursor, Ω_{ref}, was set to be 20% larger than the subject's preferred velocity of unassisted leg swing. An issue in the design of the experiments was that the transition from one experimental condition to the next one effectively introduces a change in the dynamics of the leg, and therefore requires the subject to modify his net muscle torques accordingly. Thus it was considered that randomizing the presentation of the experimental conditions would impose a strain on the subjects, and probably lead them to assume a "defensive" control strategy such as muscle co-contraction. This would be contrary to the desired effect of having the subject use the exoskeleton's dynamics to his advantage. Therefore it was decided to present the experimental factors in sequence. Five trials were executed in each of the UNCOUPLED and BASELINE conditions. Eleven trials were performed in the ASSIST condition; more trials were assigned to

this condition because it required a greater adaptation effort on the subject's part. The first trial for each experimental condition was deemed an adaptation trial and was thus dropped from the computations.

A method was developed to determine the inertia compensation gain I_c for the ASSIST trials, based on finding a threshold of instability for the coupled system formed by the human limb and the exoskeleton[3]. Every subject underwent a series of calibration trials upon completing the BASELINE trials. Subjects were instructed to swing their leg at a comfortable rhythm while wearing the exoskeleton; the duration of each calibration trial was 15 s. On each trial the subject was exposed to increasing negative values of inertia compensation gain I_c. The value of I_c employed for the ASSIST trials was the same value that, during the calibration stage, produced a first perception of increased difficulty switching the direction of the leg. The range of values of I_c thus established for the subjects in this study was was -0.12 to -0.15 kg-m^2 .

2.3.2 Subjects

Six male healthy subjects (body mass = 76.5±14.1 kg (mean ± s.d.); height = 178±6 cm; age = 21.3±1.5 years) took part in this study. None of the subjects had any previous experience using the exoskeleton. All subjects declared having no recent history of leg injuries, and all reported right-leg dominance. The experimental protocol was approved by the Institutional Review Board of Northwestern University; all subjects gave their informed consent prior to participating in the experiment. The entire protocol including obtaining informed consent, initial procedures and experimental trials was designed to last about 60 min.

2.3.3 Output variables

Figure 6 shows a time plot of the leg's RMS angular velocity Ω_h for a typical tracking trial. Also plotted is the position error of the subject's cursor, given by

$$e_x(t) = x_{ref}(t) - x_h(t) \tag{8}$$

[3]Ideally, I_c would have been made to be proportional to the moment of inertia I_h of the human limb segment. In fact, a method has been previously tested to identify I_h using the exoskeleton [24]. However, the typical estimated values of I_h (about 0.3 kg-m^2) were considerably lower than values published in the literature (0.437 kg-m^2 in Zhang [29], 0.414 kg-m^2 in Franken [30]), and therefore were not considered adequate for setting the inertia compensation gain.

where $x_{ref}(t)$ is the horizontal position of the target cursor and $x_h(t)$ is the horizontal position of the subject's cursor[4]. The present analysis will focus on the transient phase of the trial, which goes from $t = 0$ to the time t_c at which the subject's cursor catches up with the target cursor:

$$t_c \equiv t \mid_{e_x(t)=0} \tag{9}$$

The main hypothesis for the cursor-tracking experiments was that in the BASELINE trials the exoskeleton arm's inertia would cause an increase in the subjects' mean time to zero position error in comparison with the UNCOUPLED trials, but said time would decrease in the ASSIST condition due to the inertia compensation effect.

The interval for which $t > t_c$ is referred to as the "steady-state" portion of the trial, and is characterized by fairly unform RMS angular velocity on the subject's part. If the leg is assumed to follow a sinusoidal trajectory in steady state, The RMS angular velocity of leg swing, Ω_h, is given by $\Omega_h = \sqrt{2}\pi A_c f_c$, where f_c is the swing frequency in Hz and A_c is the amplitude of leg swing in radians. It must be noted that subjects were given freedom to select any combination of frequency and amplitude of swing in order to produce Ω_h. The reason is that the exoskeleton's complex impedance $Z_e^p(j\omega)$ (Figure 4) was expected to have influence on both the frequency and the amplitude of leg swing[5]. If the leg is modeled as a second-order system, the imaginary part of $Z_e^p(j\omega)$ is expected to increase the natural frequency of the human limb, and in consequence increase the selected swing frequency f_c. On the other hand, the real part of $Z_e^p(j\omega)$, which represents a negative damping term, is expected to reduce the damping ratio of the leg, which in turn can cause the swing amplitude A_c to increase.

It has to be assumed that the frequency and the amplitude of leg swing will fluctuate over the course of an experimental trial. Therefore, the method for computing the frequency and the amplitude has to accurately capture their time variations. Classic Fourier analysis is inadequate in this regard because it assumes that the time series is stationary. However, the angular trajectory of the leg during the race trial is clearly non-stationary, as it undergoes an initial transient phase. In order to determine the time variations of swing frequency, the procedure called empirical mode decomposition [31] was employed, which separates the angular

[4]Although $x_{ref}(t)$ and $x_h(t)$ correspond to horizontal distances of the user interface, nominally they have units of radians as they correspond to time integrals of RMS angular velocity.

[5]This influence can be observed even in the BASELINE condition. When subjects are allowed to swing their leg freely they tend to do so at a frequency lower than their usual frequency, but with larger amplitude.

position trajectory of the leg, $\theta(t)$, into a set of components called intrinsic mode functions (IMF). Each IMF corresponds to an oscillation mode of time-varying amplitude and frequency, but with the property of local symmetry[6]. Thus an IMF $\theta_k(t)$ will have the following general form:

$$\theta_k(t) = A_{c,k}(t) \sin\left(\frac{f_{c,k}(t)}{2\pi} t + \phi_k\right) \tag{10}$$

The instantaneous frequency $f_{c,k}(t)$ and amplitude $A_{c,k}(t)$ are computed using the Hilbert transform. The procedure is outlined in Appendix B. The present analysis focuses on the component of $\theta(t)$ with the lowest frequency range. The instantaneous frequency associated with it is considered to be the frequency of leg swing, and is denoted simply as $f_c(t)$.

2.3.4 Statistical analysis

Statistical analysis was employed to determine how the behavior of the output variables (t_c, Ω_h, f_c, A_c, e_x) changed from one experimental condition to the next. Analysis of the experimental data was performed using Matlab (The Mathworks, Natick, MA, USA). The mean values of the output variables were computed for each individual subject and each experimental condition, UNCOUPLED (U), BASELINE (B), and ASSIST (A). The first trial in each experimental condition was dropped from the computation of the mean[7]. For example, the mean times to zero position error for subject s under the different experimental conditions were given by

$$\begin{aligned}
(\bar{t_c})_s^U &= \frac{1}{N_U - 1} \sum_{i=2}^{N_U} (t_c)_{s,i}^U \\
(\bar{t_c})_s^B &= \frac{1}{N_B - 1} \sum_{i=2}^{N_B} (t_c)_{s,i}^B \\
(\bar{t_c})_s^A &= \frac{1}{N_A - 1} \sum_{i=2}^{N_A} (t_c)_{s,i}^A
\end{aligned} \tag{11}$$

For each subject, the percentage variation of the means (equations (11)) among two experimental conditions was obtained:

[6] In order to guarantee symmetry, the IMF has to satisfy two conditions: (1) the number of extrema and the number of zero crossings must either equal or differ at most by one; and (2) at any point, the mean value of the envelope defined by the local maxima and the envelope defined by the local minima is zero.

[7] Any difficulties that the subject has adapting to a new experimental condition will show especially in the first trial. Therefore this trial is not considered to be representative of the subject's overall performance for that condition.

$$
\begin{aligned}
R(\bar{t_c})_s^{U,B} &= \frac{(\bar{t_c})_s^B - (\bar{t_c})_s^U}{(\bar{t_c})_s^U} \times 100 \\
R(\bar{t_c})_s^{B,A} &= \frac{(\bar{t_c})_s^A - (\bar{t_c})_s^B}{(\bar{t_c})_s^B} \times 100 \\
R(\bar{t_c})_s^{U,A} &= \frac{(\bar{t_c})_s^A - (\bar{t_c})_s^U}{(\bar{t_c})_s^U} \times 100
\end{aligned} \tag{12}
$$

The statistics of interest were the means of the percentage variations, taken over the entire set of N_s experimental subjects:

$$
\begin{aligned}
\bar{R}(\bar{t_c})^{U,B} &= \frac{1}{N_s} \sum_{s=1}^{N_s} R(\bar{t_c})_s^{U,B} \\
\bar{R}(\bar{t_c})^{B,A} &= \frac{1}{N_s} \sum_{s=1}^{N_s} R(\bar{t_c})_s^{B,A} \\
\bar{R}(\bar{t_c})^{U,A} &= \frac{1}{N_s} \sum_{s=1}^{N_s} R(\bar{t_c})_s^{U,A}
\end{aligned} \tag{13}
$$

The standard errors of the means (s.e.m.) were also computed: $\frac{S(R(\bar{t_c})^{U,B})}{\sqrt{N_s}}$, $\frac{S(R(\bar{t_c})^{B,A})}{\sqrt{N_s}}$, $\frac{S(R(\bar{t_c})^{U,A})}{\sqrt{N_s}}$.

Analysis of variance (ANOVA) tests were performed on the output variables. The factors considered were experimental condition, subject number and number of the trial within a given experimental condition. The latter was used to detect the possible occurrence of learning or other forms of adaptation resulting from repetition of the task.

2.3.5 Catch trials

The effect of the exoskeleton's assistive forces can be confounded by subjective effects like motivation, or a tendency to overcompensate for the impedance of the exoskeleton. In order to obtain additional evidence of the exoskeleton's assistive effect, a number of catch trials were implemented for the ASSIST condition. These corresponded to trials #4, #8 and #11 of the ASSIST sequence.

Trials #4 and #8 are extended-duration trials; they are intended to show the assistive effect of the exoskeleton during the steady-state phase. Figure 7 shows exemplary plots of these catch trials for a typical ASSIST sequence. (I_c has been scaled vertically for easier visualization.) At $t = 15$ s the inertia compensation gain I_c suddenly goes to zero and remains at that value

for about 7.5 seconds, after which the original value of I_c is restored. The expected effect, noticeable in Figure 7, is a reduction in the magnitude of the leg's velocity $\Omega_h(t)$ during the time interval with $I_c = 0$, followed by a partial recovery in the magnitude of $\Omega_h(t)$ once I_c is restored. As a consequence, during the period at $I_c = 0$ the distance between the two cursors, defined by $e_x(t)$, also tends to become smaller. Trial #11 is a trial of normal duration, but with zero inertia compensation applied for the entire duration of the trial. Its main purpose is to demonstrate the effect of the exoskeleton during the transient phase. The expected behavior in this case is a slower rate of acceleration compared to inertia-compensated trials; this effect can be observed by comparing maximum RMS angular velocity for trial #11 to the corresponding value for trial #10. For every catch trial done by every subject we computed the RMS velocity ratios described in Table 1.

Trial # (tr)	RMS velocity ratios	Mean RMS velocities	Time intervals
4,8	$\frac{\bar{\Omega}_h\|_{I_c=0}}{\Omega_{h,ss}}$	$\bar{\Omega}_{h,ss} = \frac{1}{t_{fs}-t_{os}} \int_{t_{os}}^{t_{fs}} \Omega_h dt$	$t_{os} = 7.5$ s $t_{fs} = 15$ s
		$\bar{\Omega}_h\|_{I_c=0} = \frac{1}{t_{fc}-t_{oc}} \int_{t_{oc}}^{t_{fc}} \Omega_h dt$	$t_{oc} = 15$ s $t_{fc} = 22.5$ s
11	$\frac{\max(\Omega_h^{tr=11})}{\max(\Omega_h^{tr=10})}$		$t < 7.5$ s

Table 1: Computed RMS velocity ratios for catch trials.

3 Results

3.1 Transient phase

In the experiments reported here, the net time available for the subjects to adapt to the exoskeleton was rather limited. In consequence, the inertia compensation gains I_c were applied conservatively, with a range of -0.1417±0.0133 kg-m^2 (mean±s.d.). Thus the net inertia value of 0.22 kg-m^2 was not fully compensated for.

Figure 8 shows the percentage variations in the time to zero position error t_c during the tracking task. The experimental condition (UNCOUPLED, BASELINE, ASSIST) had a significant effect ($p = 0.007$) on this catch-up time. For the BASELINE condition, the time to zero position error had an increase of 41.7±21.2% (mean±s.e.m.) with respect to the UNCOUPLED condition. Such increase is due almost certainly to the exoskeleton's arm inertia, which naturally limits the angular acceleration that can be imparted on the leg. By contrast, the mean time to

zero position error in the ASSIST condition was only 19.0% higher than in the UNCOUPLED condition, although with 15.3% s.e.m. Therefore, emulated inertia compensation in the ASSIST condition counteracted to a certain extent the effects of the arm's inertia, although not to the point of making the subjects match their times for the UNCOUPLED case.

The trial number within a particular experimental condition was not found to be a significant factor on the time to to catch-up ($p = 0.508$). Thus the experiment did not reveal effects deriving from repetition of the task. However, longer series of trials may be necessary to determine conclusively whether repetition is a factor on the subjects' performance, for example through learning or subject fatigue.

The general behavior of the RMS velocity as a function of time during the tracking experiment is shown in Figure 9(a). The plots provide comparisons of ASSIST vs. UNCOUPLED condition, and ASSIST vs. BASELINE. The time trajectories show an initial high-velocity phase during which subjects tried to reach the target cursor, followed by a "steady-state" phase characterized by roughly constant RMS angular velocity. In order to achieve greater angular velocity during the transient phase, subjects tended to impart a combination of large swing frequency (Figure 9(b)), and large swing amplitude (Figure 9(c)). A precise estimate of the effects of the experimental conditions was obtained by first computing, for each trial, the mean values of RMS angular velocity, swing frequency and swing amplitude during the transient phase:

$$\begin{aligned} \Omega_{h,tr} &= \frac{1}{t_c}\int_0^{t_c} \Omega_h dt \\ f_{c,tr} &= \frac{1}{t_c}\int_0^{t_c} f_c dt \\ A_{c,tr} &= \frac{1}{t_c}\int_0^{t_c} A_c dt \end{aligned} \tag{14}$$

The percentage variations of mean RMS angular velocity among experimental conditions ($\bar{R}(\bar{\Omega}_{h,tr})^{U,B}$, $\bar{R}(\bar{\Omega}_{h,tr})^{B,A}$, $\bar{R}(\bar{\Omega}_{h,tr})^{U,A}$) were computed in a manner analogous to the one described by equations (11), (12) and (13). A similar procedure was followed for the mean swing frequency and the mean swing amplitude. The results are shown in Figure 10. The experimental condition was found to have a significant effect ($p \simeq 0$) on all the computed percentage variations. The behavior of the RMS velocity basically reflected the behavior of the swing frequency (Figures 10(a) and 10(b)). In the BASELINE condition subjects reduced their swing frequency

in comparison with the UNCOUPLED condition, which is consistent with the increased inertia introduced by the exoskeleton's mechanism. The ASSIST condition produced a moderate recovery in swing frequency. The effect of the experimental conditions on the swing amplitude (Figure 10(c)) was less discernible.

The time histories of the position error $e_x(t)$ provide another perspective on the effect of the exoskeleton on the legs' transient response. Figure 11 shows the averaged time histories of $e_x(t)$ for all subjects under each experimental condition. In the BASELINE condition, the position error converges to steady state more slowly. In the ASSIST condition there appears to be a similar rate of convergence together with non-zero steady-state error. The shape of the error curves suggests that the subject's response when tracking the reference cursor can be modeled as a second-order system. Thus the transfer function relating the position error $e_x(t)$ to the target cursor's position $x_{ref}(t)$ is defined as

$$F_E(s) \equiv \frac{E(s)}{X_{ref}(s)} \tag{15}$$

In the tracking experiment, the position of the target cursor is given by $x_{ref}(t) = \Omega_{ref} t$. The error response to this ramp input in the Laplace domain is

$$E(s) = \Omega_{ref} \frac{F_E(s)}{s^2} \tag{16}$$

From the final value theorem, the steady-state value of the position error is given by

$$\lim_{t \to \infty} e_x(t) = \Omega_{ref} \lim_{s \to 0} \frac{F_E(s)}{s} \tag{17}$$

In order to reproduce the steady-state error behaviors shown in Figure 11, the following realization of $F_E(s)$ is proposed:

$$F_E(s) = K_E \frac{s(s + \alpha_E)}{s^2 + 2\zeta_E \omega_{n,E} s + \omega_{n,E}^2} \tag{18}$$

The value of the steady-state error in equation (18) is controlled by the term α_E. Figure 11 suggests that, for the UNCOUPLED and BASELINE conditions, α_E should be nearly zero, but clearly negative in the ASSIST condition. For every trial done by every subject, the parameters ζ_E, $\omega_{n,E}$, α_E and K_E of the position error response were identified using Matlab's `fminsearch` optimization function. The decay rate of the error response was computed as

$$\sigma_E = \zeta_E \omega_{n,E} \tag{19}$$

This decay rate indicates how fast the position error converges towards steady state.

Figure 12(a) shows the percentage variations of the decay rate of the error among experimental conditions. There was not a distinguishable effect of the experimental conditions on the decay rate ($p = 0.582$). Thus it appears that the ASSIST condition (inertia compensation) did not contribute to increase the rate of convergence of the position error. On the other hand, Figure 12(b) shows that the ASSIST condition produced a right-plane zero (α_E) of large magnitude ($p = 0.044$). This zero reflects the tendency of the subjects to overshoot the target cursor in the ASSIST condition, which can be noticed in Figure 11(c). Thus equation (18) suggests that the error response in the ASSIST condition corresponds to a non-minimum phase system. The non-passive behavior of the system can probably be explained by the exoskeleton producing a net transfer of energy to the leg during the trial.

3.2 Steady-state phase

The steady-state phase of the task provided information about the subjects' ability to perform a moderately challenging precision task, namely tracking the position of the target cursor, under the different experimental conditions. For each trial performed by every subject, the RMS value of the position error $e_x(t)$ was computed for $t > t_c$. Figure 13 shows the mean percentage variations of the RMS position error among experimental conditions. Position error increased significantly in the BASELINE condition and more so in the ASSIST condition ($p \simeq 0$), which suggests that subjects had more difficulty tracking the target when using the exoskeleton.

3.3 Catch trials

The removal of inertia compensation had a highly significant effect on the RMS velocity of swing ($p = 0.034$). Figure 14 shows the mean ratios of RMS velocity for trials #4 and #8 in the ASSIST condition, computed in the way described in Table 1. Error bars show the standard error of the mean. The ratio of maximum RMS angular velocities between trials #11 and #10 was 0.96±0.02% (mean±s.e.m.). Thus the removal of inertia compensation was found to reduce the subjects' capability to accelerate the leg, even though they may have compensated for the exoskeleton's inertia during trial #11.

4 Discussion

4.1 Control method based on emulated inertia compensation

A major challenge in enabling an exoskeleton to increase the agility of the limbs is counteracting the mechanism's inertia. The solution proposed here was a controller that combines admittance control and positive feedback of low-pass filtered acceleration. For its first implementation, the controller was tested on a 1-DOF, statically mounted exoskeleton that assists knee flexion and extension. The use of positive acceleration feedback makes the exoskeleton behave as an active impedance. To the best of the author's knowledge, the experiments reported here are among the first in which active impedance has been employed specifically to assist the swing movement of the limbs.

Robot passivity has been long established as a condition for guaranteed coupled stability in human-robot interaction [32, 33]. By contrast, the control method presented here makes the exoskeleton non-passive, with the implication that the exoskeleton is unstable in isolation. Stable interaction between the exoskeleton and the lower extremities is possible due in part to the passive dynamics of the leg, but it is very likely that the human sensorimotor control plays an important role in stabilizing the coupled system [34]. In the experiments reported here, subjects were generally quite able to interact stably with the exoskeleton. A similar ability was observed in a previous study in which the exoskeleton's controller displayed pure negative damping [23].

4.2 Tracking task: transient phase

The present study sought to determine whether emulated inertia compensation can improve the subject's ability to execute leg movements requiring high accelerations. The tracking task required subjects to increase the mean speed of the leg as quickly as possible. In the BASELINE condition, the exoskeleton mechanism's inertia slowed down the leg's response, which resulted in longer times to catch up with the target. Emulated inertia compensation in the ASSIST condition produced a moderate improvement in the subjects' catch-up times, although they were not quite able to match the times of the UNASSISTED case. The latter outcome was not unexpected, considering that the inertia compensation gains did not fully compensate the inertia of the exoskeleton's arm. In order to improve the speed of reactive movements with respect to those of the unassisted leg, it may be necessary to expose subjects to higher magnitudes of

negative compensation gain I_c, which in turn will probably require longer adaptation periods. However, it should be noted that the control algorithm produces two coupled effects: modulation of the natural frequency of the leg, and net energy transfer to the leg. The latter is due to the negative damping term of the port impedance ($Re\{Z_e^p(j\omega_c)\}$ in Figure 3). Thus the controller can in principle have an assistive effect on the user even when the exoskeleton's inertia is not fully compensated.

The variations in the time to zero position error among experimental conditions (Figure 8) were consistent with the observed variations in swing frequency (Figure 10(b)). These were in turn consistent with the inertia compensation gains employed. However, when the behavior of the position error of the tracking experiment was analyzed as a second-order system, the ASSIST condition did not increase the rate of decay of the error toward steady state, as would have been expected from a system with reduced inertia. Instead it was found that the work performed by negative damping in the ASSIST condition made itself apparent in the fact that subjects tended to overshoot the target and remain ahead of it (Figure 11(c)). For future experiments it would be desirable to establish a relationship between work performed by negative damping and muscle activation.

4.3 Tracking task: steady-state phase

A complementary effect of inertia compensation is that it contributes to increase the steady-state frequency of leg swing. In a previous study with the 1-DOF exoskeleton [25], subjects were not constrained to track the target cursor, but merely to move their cursor past the target within a certain period of time. In the ASSIST condition, subjects settled on a swing frequency noticeably higher than that of the BASELINE condition. A similar trend was observed in the experiments reported here (Figure 9(b)). On the other hand, the steady-state RMS position error was consistently highest in the ASSIST condition, which indicates that subjects had difficulty maintaining alignment between their cursor and the target cursor. The probable cause is that, since the exoskeleton's complex impedance has influence on both the frequency and the amplitude of leg swing, as pointed out in Sections 2.2.3 and 2.3.3, it was probably difficult for subjects to control their amplitude and frequency of leg swing independently.

It is possible that the exoskeleton induces a preferable combination of swing frequency and swing amplitude, for example one that minimizes metabolic cost, and in consequence a preferable value of RMS angular velocity as well. If that is the case, swinging at lower speeds may be

actually more difficult by demanding more metabolic energy. It remains to be determined whether this difficulty can be overcome through longer training sessions using the exoskeleton.

4.4 Tracking task: catch trials

Catch trials provided complementary evidence of the assistive effect of the exoskeleton. Sudden removal of inertia compensation (i.e. making $I_c = 0$) consistently produced a moderate reduction in RMS angular velocity, in both the transient and steady-state phases of the trials. However, for a more objective measurement of the assistive effect of the exoskeleton, future experiments will need to measure the net torque and net work contributed by the exoskeleton and by the muscles.

4.5 Future work

A planned next step in this research is to test the emulated inertia compensation method on a wearable exoskeleton for assisting the swing phase of walking. Muscle activation during the swing phase occurs mainly in the hip flexor muscles [35]. Thus the design being considered is a hip-mounted device with actuators assisting hip flexion and extension in the sagittal plane. An hypothesis to be tested is whether emulated inertia compensation leads to an increase in the preferred step frequency, and by extension the speed of walking, without significantly increasing metabolic cost.

Each phase of the walking cycle contributes to the overall metabolic cost. At normal speeds, the metabolic cost of the stance phase represents about 45% of the total cost, whereas leg swing is relatively inexpensive [36]. However, as step frequency increases, the relative contribution of leg swing to the metabolic cost tends to surpass that of the stance phase, reaching nearly 40% of the total cost at speeds near the walk-to-run transition value [37]. Therefore, an exoskeleton that acts chiefly during the swing phase is better suited to enabling walking at higher speeds.

However, it will be necessary to determine how the energetic cost of leg swing trades off against the energetic cost of step-to-step transitions when wearing the exoskeleton. The negative damping term in the exoskeleton's impedance (Figure 4) will likely contribute to increase step length. However, increased step length may increase the cost of redirecting the center of mass during step to step transitions [38]. The current version of the exoskeleton controller has only one adjustable gain, I_c which prevents adjusting the pendulum frequency and positive work effects independently. For walking assistance the control algorithm will probably need to tune

these effects separately.

A second research question is whether emulated inertia compensation can help the user perform faster reactive movements, like corrective stepping in order to avoid a fall. The experimental results reported here suggest this might be the case. The question could be answered through an experiment similar the hip-perturbation experiment reported by Thelen [39]. It was found that the ability to regain balance declines with age, due mainly to a reduction in capability to produce joint torques. Likewise, experiments reported by Dean [40] revealed that maximum isometric hip torque decreases significantly with age. An exoskeleton with inertia compensation might be able to compensate for the lost capability to produce muscle force, by making the leg's dynamics more responsive to the muscle torques that the subject can generate.

5 Conclusions

A study was conducted to test a novel exoskeleton control method aimed at increasing the agility of the lower limbs. The controller was designed to make the 1-DOF exoskeleton unstable in isolation, but capable of interacting stably with the user on account of the passive dynamics of the human limb. The experimental results suggest that emulated inertia compensation can counteract the adverse effects of the exoskeleton's inertia on the transient response of the human limbs. In steady state, the controller's effect was an increase in the frequency of leg swing with respect to the unassisted case. The experiments also produced evidence of the controller's capability to transfer net energy to the limbs. Catch trials showed that the observed differences among experimental conditions were not due solely to subjective factors. With larger feedback gains and sufficient adaptation time, the controller may enable exoskeleton users to perform reactive movements that are consistently faster than in the unassisted case. So far the controller has only been tested at the single-joint level. A logical next step will be to test the emulated inertia compensation method on a wearable exoskeleton designed to assist walking. An appropriate research question is whether the controller can help users to take quicker steps in response to destabilizing perturbations.

6 Acknowledgements

This work was supported by a grant form the Honda Research Institute (Mountain View, CA).

A Notation

- $A_c(t)$ = Instantaneous amplitude of leg swing (rad).
- b_{arm} = Damping of the exoskeleton's arm (N-m-s/rad).
- $\bar{b}_e^d$ = Virtual (admittance-model) damping of the exoskeleton's drive mechanism at the torque sensor port (N-m-s/rad).
- $e_x(t)$ = Position error of the subject's cursor (rad).
- $f_c(t)$ = Instantaneous frequency of leg swing (Hz).
- I_{arm} = Moment of inertia of the exoskeleton's arm (kg-m^2).
- I_c = Emulated inertia compensator's gain (kg-m^2).
- I_h = Moment of inertia of the human limb (kg-m^2).
- $\bar{I}_e^d$ = Virtual (admittance-model) moment of inertia of the exoskeleton's drive mechanism at the torque sensor port (kg-m^2).
- k_{arm} = Gravitational spring constant of the exoskeleton's arm (N-m/rad).
- $\bar{k}_e^d$ = Virtual (admittance-model) stiffness of the exoskeleton's drive mechanism at the torque sensor port (N-m/rad).
- t_c = Time to zero position error (s).
- $x_h(t)$ = Horizontal position of the subject's cursor (rad).
- $x_{ref}(t)$ = Horizontal position of the target cursor in the tracking trial (rad).
- $Z_e^p(j\omega_c)$ = Closed-loop impedance of the exoskeleton at the port of interaction with the user (N-m-s/rad)
- α_E = Zero of the position-error response of the human leg in the tracking trial (rad).
- $\theta(t)$ = Angular position of the exoskeleton arm (rad).
- σ_E = Decay rate of the position-error response of the human leg in the tracking trial (1/s).
- τ_s = Torque measured by the exoskeleton's torque sensor (N-m).

- ω_c = Angular frequency of leg swing (rad/s).
- $\omega_{n,e}$ = Natural frequency of the exoskeleton drive (rad/s).
- $\Omega_h(t)$ = RMS angular velocity of swing of the human limb (rad/s).
- Ω_{ref} = Reference RMS angular velocity for the tracking trial (rad/s).

B Computation of the instantaneous frequency and amplitude of a signal using the Hilbert spectrum

For an arbitrary time series $x(t)$, the Hilbert transform $y(t)$ is defined as the convolution of $x(t)$ with t^{-1}:

$$y(t) = \frac{1}{\pi} P \int_{-\infty}^{\infty} \frac{x(t')}{t - t'} dt' \tag{20}$$

where P denotes the Cauchy principal value [8]. With the above definition, $x(t)$ and $y(t)$ are combined to form a complex conjugate pair yielding the analytic signal $z(t)$:

$$z(t) = x(t) + iy(t) = a(t)e^{i\phi(t)} \tag{21}$$

where

$$a(t) = \left[x^2(t) + y^2(t)\right]^{\frac{1}{2}} \tag{22}$$

and

$$\phi(t) = \arctan \frac{y(t)}{x(t)} \tag{23}$$

From (23) the instantaneous frequency of $x(t)$ is defined as

$$\omega(t) = \frac{d\phi}{dt} \tag{24}$$

whereas the instantaneous amplitude is defined precisely by (22).

[8] The Cauchy principal value of $f(x)$ is defined [41] as

$$\lim_{\alpha \to \infty} \int_{-\alpha}^{\alpha} f(x) dx$$

In order to determine the instantaneous frequency and amplitude of the subject's leg motions, the leg's angular position signal $\theta(t)$ was decomposed into a set of components called intrinsic mode functions (IMF), following the procedure called empirical mode decomposition [31]. Each IMF corresponds to an oscillation mode of variable amplitude and frequency, but with the property of local symmetry. For the purposes of this analysis, the instantaneous amplitude and frequency of interest are those corresponding to the component of $\theta(t)$ with the lowest range of instantaneous frequency. The mode of interest was converted to an analytic signal by obtaining the Hilbert transform. The instantaneous swing amplitude A_s and swing frequency ω_c were determined by applying (22) and (24) respectively to the computed Hilbert transform.

References

[1] Kazerooni H, Racine JL, Huang L, Steger R. On the Control of the Berkeley Lower Extremity Exoskeleton (BLEEX). In: Robotics and Automation, 2005. ICRA 2005. Proceedings of the 2005 IEEE International Conference on; 2005. p. 4353 – 4360.

[2] Walsh CJ, Paluska D, Pasch K, Grand W, Valiente A, Herr H. Development of a lightweight, underactuated exoskeleton for load-carrying augmentation. In: Robotics and Automation, 2006. ICRA 2006. Proceedings 2006 IEEE International Conference on; 2006. p. 3485 –3491.

[3] Kawamoto H, Lee S, Kanbe S, Sankai Y. Power assist method for HAL-3 using EMG-based feedback controller. In: Systems, Man and Cybernetics, 2003. IEEE International Conference on. vol. 2; 2003. p. 1648 – 1653 vol.2.

[4] Lee S, Sankai Y. Virtual impedance adjustment in unconstrained motion for an exoskeletal robot assisting the lower limb. Advanced Robotics. 2005;19(7):773–795.

[5] Lee S, Sankai Y. Power assist control for walking aid with HAL-3 based on EMG and impedance adjustment around knee joint. In: Intelligent Robots and Systems, 2002. IEEE/RSJ International Conference on. vol. 2; 2002. p. 1499 – 1504 vol.2.

[6] Jezernik S, Colombo G, Morari M. Automatic gait-pattern adaptation algorithms for rehabilitation with a 4-DOF robotic orthosis. IEEE Transactions on Robotics and Automation. 2004;20(3):574–582.

[7] Banala SK, Kim SH, Agrawal SK, Scholz JP. Robot Assisted Gait Training With Active Leg Exoskeleton (ALEX). Neural Systems and Rehabilitation Engineering, IEEE Transactions on. 2009 Feb;17(1):2–8.

[8] Veneman JF, Kruidhof R, Hekman EEG, Ekkelenkamp R, Van Asseldonk EHF, van der Kooij H. Design and Evaluation of the LOPES Exoskeleton Robot for Interactive Gait Rehabilitation. Neural Systems and Rehabilitation Engineering, IEEE Transactions on. 2007 Sept;15(3):379–386.

[9] Ferris DP, Czerniecki JM, Hannaford B. An Ankle-Foot Orthosis Powered by Artificial Pneumatic Muscles. Journal of Applied Biomechanics. 2005;21:189–197.

[10] Sawicki GS, Ferris DP. Mechanics and energetics of level walking with powered ankle exoskeletons. Journal of Experimental Biology. 2008;211:1402–1413.

[11] Blaya JA, Herr H. Adaptive Control of a Variable-Impedance Ankle-Foot Orthosis to Assist Drop-Foot Gait. Neural Systems and Rehabilitation Engineering, IEEE Transactions on. 2004;12(1):24–31.

[12] Pratt JE, Krupp BT, Morse CJ, Collins SH. The RoboKnee: an exoskeleton for enhancing strength and endurance during walking. In: Robotics and Automation, 2004. Proceedings. ICRA '04. 2004 IEEE International Conference on. vol. 3; 2004. p. 2430 – 2435 Vol.3.

[13] Ferris D, Sawicki G, Domingo A. Powered Lower Limb Orthoses for Gait Rehabilitation. Top Spinal Cord Inj Rehabil. 2005;11(2):34–49.

[14] Dollar A, Herr H. Lower Extremity Exoskeletons and Active Orthoses: Challenges and State of the Art. IEEE Transactions on Robotics. 2008;24(1):144–158.

[15] Kuo AD. A Simple Model of Bipedal Walking Predicts the Preferred Speed–Step Length Relationship. Journal of Biomechanical Engineering. 2001;123(3):264–269.

[16] Uemura M, Kanaoka K, Kawamura S. Power Assist Systems based on Resonance of Passive Elements. In: Intelligent Robots and Systems, 2006 IEEE/RSJ International Conference on; 2006. p. 4316 –4321.

[17] Newman WS. Stability and Performance Limits of Interaction Controllers. Journal of Dynamic Systems, Measurement, and Control. 1992;114(4):563–570.

[18] Buerger SP, Hogan N. Complementary Stability and Loop Shaping for Improved Human-Robot Interaction. Robotics, IEEE Transactions on. 2007;23(2):232–244.

[19] Browning RC, Modica JR, Kram R, Goswami A. The Effects of Adding Mass to the Legs on the Energetics and Biomechanics of Walking. Medicine and Science in Sports and Exercise. 2007;39(3):515–525.

[20] Royer TD, Martin PE. Manipulations of Leg Mass and Moment of Inertia: Effects on Energy Cost of Walking. Medicine and Science in Sports and Exercise. 2005;37(4):649–656.

[21] Melzer I, Oddsson LIE. The Effect of a Cognitive Task on Voluntary Step Execution in Healthy Elderly and Young Individuals. Journal of the American Geriatrics Society. 2004;52(8):1255–1262.

[22] Aguirre-Ollinger G, Colgate JE, Peshkin MA, Goswami A. Active-Impedance Control of a Lower-Limb Assistive Exoskeleton. In: Rehabilitation Robotics, 2007. ICORR 2007. IEEE 10th International Conference on; 2007. p. 188 –195.

[23] Aguirre-Ollinger G, Colgate JE, Peshkin MA, Goswami A. A 1-DOF assistive exoskeleton with virtual negative damping: effects on the kinematic response of the lower limbs. In: Intelligent Robots and Systems, 2007. IROS 2007. IEEE/RSJ International Conference on; 2007. p. 1938 –1944.

[24] Aguirre-Ollinger G. Active Impedance Control of a Lower-Limb Assistive Exoskeleton [dissertation]. Northwestern University. Evanston, IL; 2009.

[25] Aguirre-Ollinger G, Colgate JE, Peshkin MA, Goswami A. Design of an Active 1-DOF Lower-Limb Exoskeleton with Inertia Compensation [in revision]. The International Journal of Robotics Research. 2010;.

[26] Stengel RF. Optimal Control and Estimation. New York, NY: Dover Publications, Inc.; 1994.

[27] Brown RL. Error behaviour of multistep methods applied to unstable differential systems. Applied Mathematical Modelling. 1978;2(2):115–118.

[28] Rapaport DC. The Art of Molecular Dynamics Simulation. 2nd ed. Cambridge, UK: Cambridge University Press; 2004.

[29] Zhang LQ, Nuber G, Butler J, Bowen M, Rymer WZ. In Vivo Human Knee Joint Dynamic Properties as Functions of Muscle Contraction and Joint Position. Journal of Biomechanics. 1998;31:71–76.

[30] Franken HM, Veltink PH, Tijsmans R, Nijmeijer H, Boom HBK. Identification of Passive Knee Joint and Shank Dynamics in Paraplegics Using Quadriceps Stimulation. IEEE Transactions on Rehabilitation Engineering;1(3):154.

[31] Huang NE, Shen Z, Long SR, Wu MC, Shih HH, Zheng Q, et al. The empirical mode decomposition and the Hilbert spectrum for nonlinear and non-stationary time series analysis. Proc R Soc Lond A. 1998;454:903–995.

[32] Colgate E, Hogan N. The Interaction of Robots with Passive Environments: Application to Force Feedback Control. Fourth International Conference on Advanced Robotics. 1989;.

[33] Colgate JE, Hogan N. Robust Control of Dynamically Interacting Systems. International Journal of Control. 1988;48(1):65–88.

[34] Burdet E, Osu R, Franklin DW, Milner TE, Kawato M. The central nervous system stabilizes unstable dynamics by learning optimal impedance. Nature. 2001;414:446–449.

[35] Gottschall JS, Kram R. Energy cost and muscular activity required for leg swing during walking. Journal of Applied Physiology. 2005;99:23–30.

[36] Grabowski A, Farley CT, Kram R. Independent metabolic costs of supporting body weight and accelerating body mass during walking. Journal of Applied Physiology. 2005;98:579–583.

[37] Doke J. On the Preferred Step Frequencies of Walking: Mechanics and Energetics of Swinging the Human Leg [dissertation]. University of Michigan. Ann Arbor, MI, USA; 2005.

[38] Donelan JM, Kram R, Kuo AD. Mechanical work for step-to-step transitions is a major determinant of the metabolic cost of human walking. Journal of Experimental Biology. 2002;205:3717–3727.

[39] Thelen D, Wojcik L, Schultz A, Ashton-Miller J, Alexander N. Age differences in using a rapid step to regain balance during a forward fall. Journal of Gerontology: Medical Sciences. 1999;52A(1):M8–M13.

[40] Dean JC, Kuo AD, Alexander NB. Age-Related Changes in Maximal Hip Strength and Movement Speed. The Journals of Gerontology: Series A : Biological sciences and medical sciences. 2004;59A(3):286–292.

[41] Kanwal RP. Linear Integral Equations: Theory and Technique. 2nd ed. Boston: Birkhauser; 1996.

List of Figures

1 Diagram of the 1-DOF exoskeleton's motor, cable drive and arm assembly. 31

2 Statically mounted 1-DOF exoskeleton for knee flexion and extension. 32

3 Detailed model of the exoskeleton controller. A virtual admittance model generates a reference state trajectory $\mathbf{q}_{ref}$. The input to the admittance model is the sum of the torque sensor measurement τ_s plus the feedback torque from the inertia compensator. The reference trajectory $\mathbf{q}_{ref}$ is tracked by a closed-loop controller that uses an LQ regulator. The exoskeleton drive outputs are the angular velocity w_m of the servo motor reflected on the output shaft, and the output shaft's own angular velocity w_s. The exoskeleton's arm angle θ is measured by a proprietary feedback device that emulates an encoder. A state observer with a Kalman filter is employed to compute a full state estimate for feedback. In the inertia compensator, the angular acceleration feedback signal is low-pass filtered by a fourth-order Butterworth filter ($H_{lo}(s)$) with a cutoff frequency of 4 Hz. A negative feedback gain I_c emulates a negative inertia term at low frequencies. . 33

4 Parametric plots of the exoskeleton's closed-loop impedance at the interaction port, $Z_e^p(j\omega_c)$, where $\omega_c = 2\pi f_c$ and f_c is the leg swing frequency in Hz. Inertia compensation gains are expressed as fractions of the exoskeleton's net inertia $\bar{I}_e = I_e^d + I_{arm}$. 34

5 Graphic user interface for the exoskeleton-based tracking task. The subject sees only the cursors and the "scrolling" field. 35

6 Example of a time trajectory for the tracking trial. The plot shows the evolution of the RMS angular velocity of leg swing, Ω_h, when tracking a the reference value Ω_{ref}. Also shown is the time trajectory of the position error $e_x(t)$ 36

7 Time series plots of typical catch trials for the ASSIST task with inertia compensation. The time plot for the inertia compensation gain I_c has been scaled vertically for easier visualization. 37

8 Percentage variations (mean ± s.e.m.) for the time to zero position error (t_c), among the different experimental conditions: BASELINE vs. UNCOUPLED ($\bar{R}(\bar{t_c})^{U,B}$), ASSIST vs. BASELINE ($\bar{R}(\bar{t_c})^{B,A}$), and ASSIST vs. UNCOUPLED ($\bar{R}(\bar{t_c})^{U,A}$). 38

9 Time trajectories of the kinematic variables during the tracking task: (a) RMS angular velocity, (b) swing frequency, (c) swing amplitude. Line plots represent the mean values across all subjects and all trials within a particular experimental condition. Shaded regions represent the standard error of the mean. 39

10 Transient phase: percentage variations (mean ± s.e.m.) among the different experimental conditions for (a) mean RMS angular velocity ($\Omega_{h,tr}$), (b) mean swing frequency ($f_{c,tr}$) and (c) mean swing amplitude ($A_{c,tr}$). 40

11 Averaged time histories of the position error $e_x(t)$, for the different experimental conditions: (a) UNCOUPLED, (b) BASELINE, (c) ASSIST. Plotted data are mean (lines) ± s.e.m. (shaded regions) of $e_x(t)$. The theoretical mean times for zero position error (zero-crossings of the horizontal axis) are also shown. 41

12 Position-error response modeled as a second-order system. (a) Percentage variations of the decay rate of the position error (σ_E) among the different experimental conditions: BASELINE vs. UNCOUPLED ($\bar{R}(\bar{\sigma_E})^{U,B}$), ASSIST vs. BASELINE ($\bar{R}(\bar{\sigma_E})^{B,A}$), and ASSIST vs. UNCOUPLED ($\bar{R}(\bar{\sigma_E})^{U,A}$). (b) Mean ± s.e.m. of the second-order system's zero (α_E) for each experimental condition. 42

13 Percentage variations (mean ± s.e.m.) for the RMS position error during the steady-state phase, among the different experimental conditions: BASELINE vs. UNCOUPLED, ASSIST vs. BASELINE, and ASSIST vs. UNCOUPLED 43

14 Mean ratios of RMS velocity for catch trials #4 and #8 in the ASSIST condition. 44

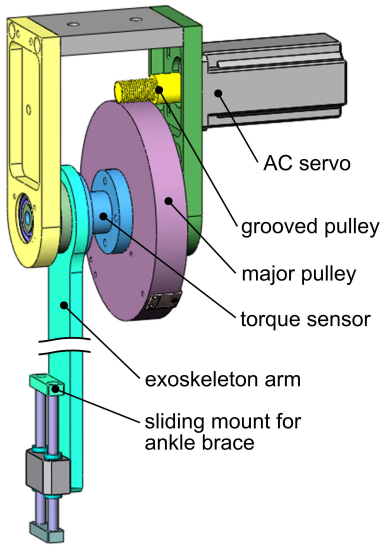

Figure 1: Diagram of the 1-DOF exoskeleton's motor, cable drive and arm assembly.

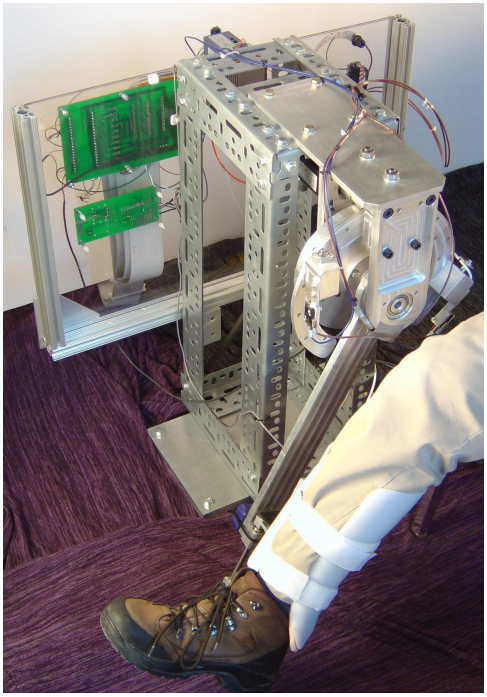

Figure 2: Statically mounted 1-DOF exoskeleton for knee flexion and extension.

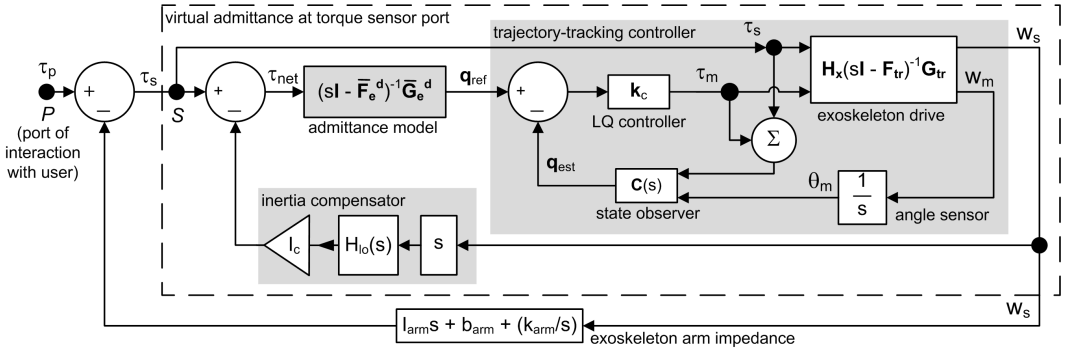

Figure 3: Detailed model of the exoskeleton controller. A virtual admittance model generates a reference state trajectory $\mathbf{q}_{ref}$. The input to the admittance model is the sum of the torque sensor measurement τ_s plus the feedback torque from the inertia compensator. The reference trajectory $\mathbf{q}_{ref}$ is tracked by a closed-loop controller that uses an LQ regulator. The exoskeleton drive outputs are the angular velocity w_m of the servo motor reflected on the output shaft, and the output shaft's own angular velocity w_s. The exoskeleton's arm angle θ is measured by a proprietary feedback device that emulates an encoder. A state observer with a Kalman filter is employed to compute a full state estimate for feedback. In the inertia compensator, the angular acceleration feedback signal is low-pass filtered by a fourth-order Butterworth filter ($H_{lo}(s)$) with a cutoff frequency of 4 Hz. A negative feedback gain I_c emulates a negative inertia term at low frequencies.

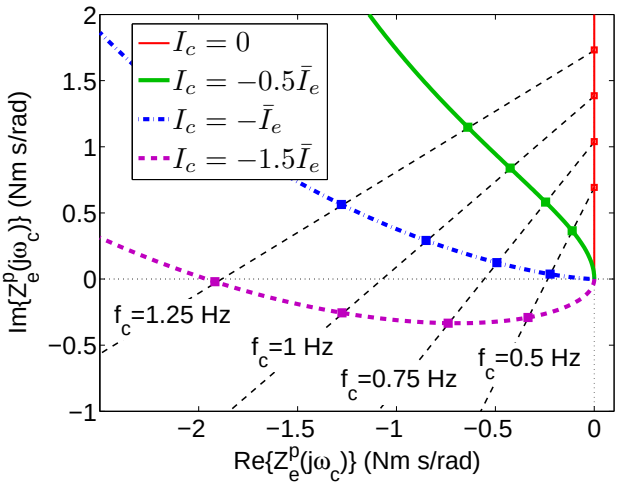

Figure 4: Parametric plots of the exoskeleton's closed-loop impedance at the interaction port, $Z_e^p(j\omega_c)$, where $\omega_c = 2\pi f_c$ and f_c is the leg swing frequency in Hz. Inertia compensation gains are expressed as fractions of the exoskeleton's net inertia $\bar{I}_e = I_e^d + I_{arm}$.

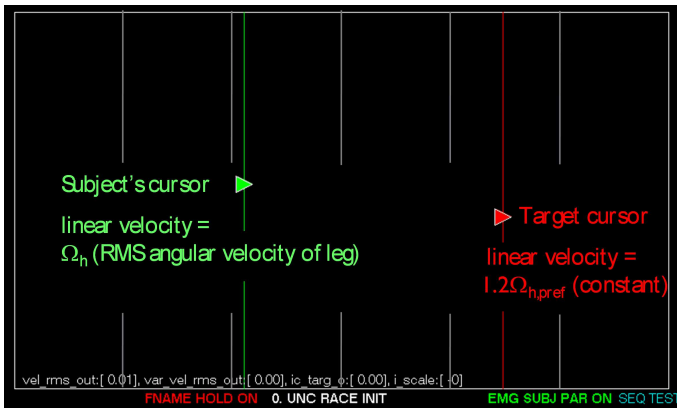

Figure 5: Graphic user interface for the exoskeleton-based tracking task. The subject sees only the cursors and the "scrolling" field.

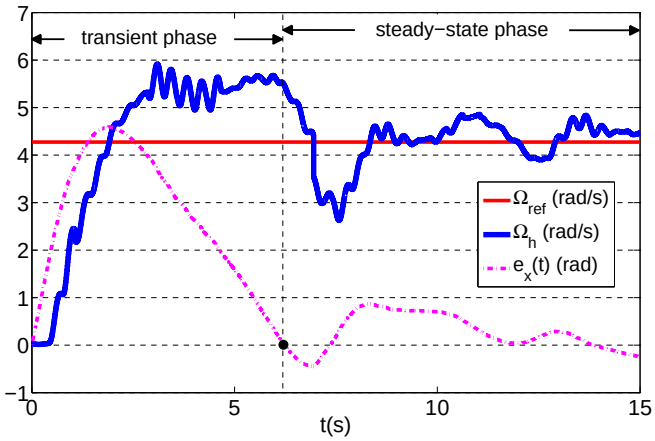

Figure 6: Example of a time trajectory for the tracking trial. The plot shows the evolution of the RMS angular velocity of leg swing, Ω_h, when tracking a the reference value Ω_{ref}. Also shown is the time trajectory of the position error $e_x(t)$.

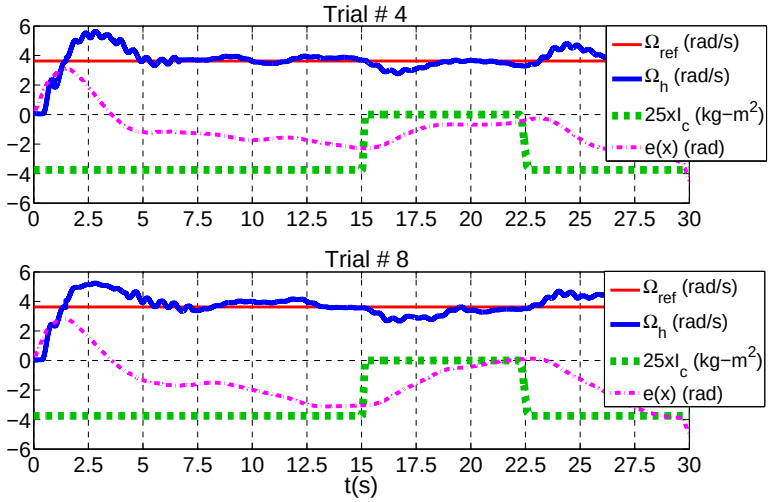

Figure 7: Time series plots of typical catch trials for the ASSIST task with inertia compensation. The time plot for the inertia compensation gain I_c has been scaled vertically for easier visualization.

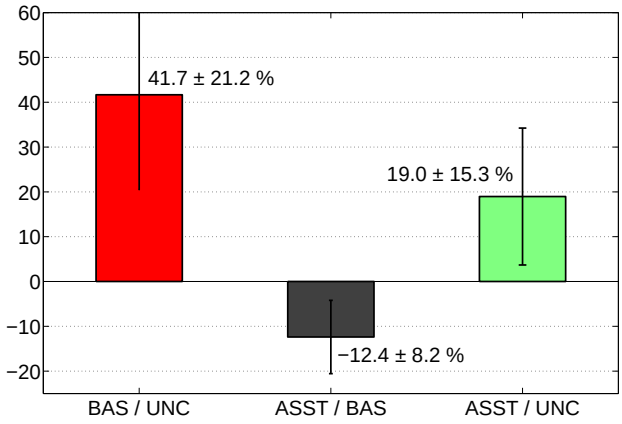

Figure 8: Percentage variations (mean ± s.e.m.) for the time to zero position error (t_c), among the different experimental conditions: BASELINE vs. UNCOUPLED ($\bar{R}(\bar{t_c})^{U,B}$), ASSIST vs. BASELINE ($\bar{R}(\bar{t_c})^{B,A}$), and ASSIST vs. UNCOUPLED ($\bar{R}(\bar{t_c})^{U,A}$).

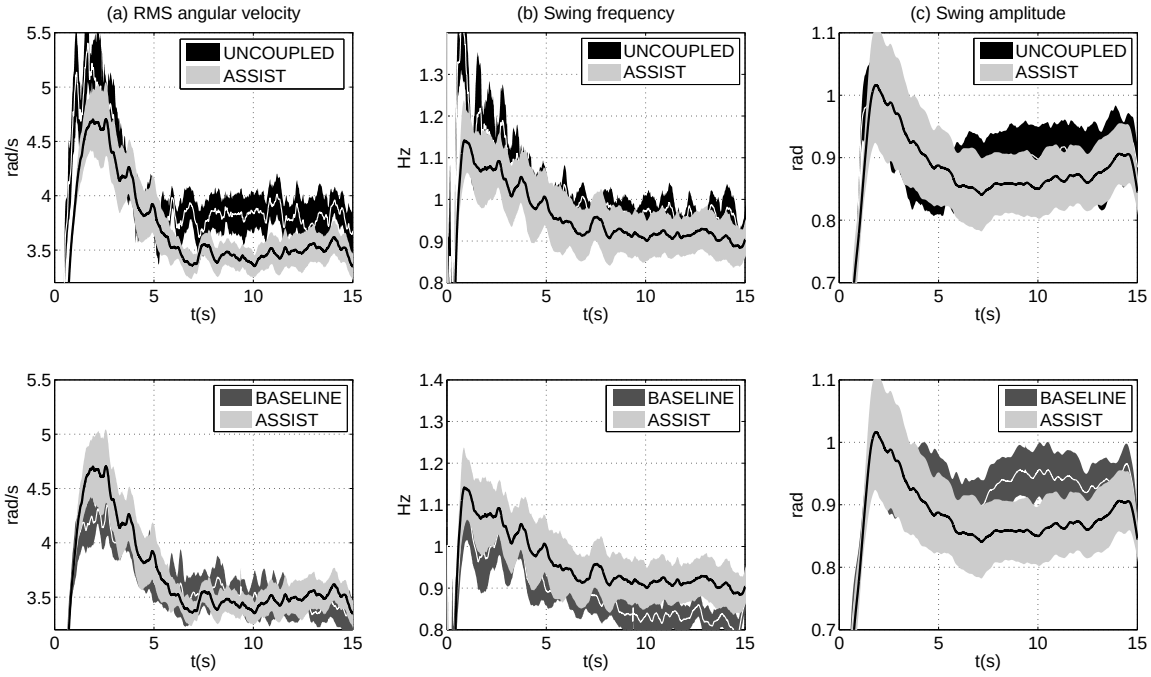

Figure 9: Time trajectories of the kinematic variables during the tracking task: (a) RMS angular velocity, (b) swing frequency, (c) swing amplitude. Line plots represent the mean values across all subjects and all trials within a particular experimental condition. Shaded regions represent the standard error of the mean.

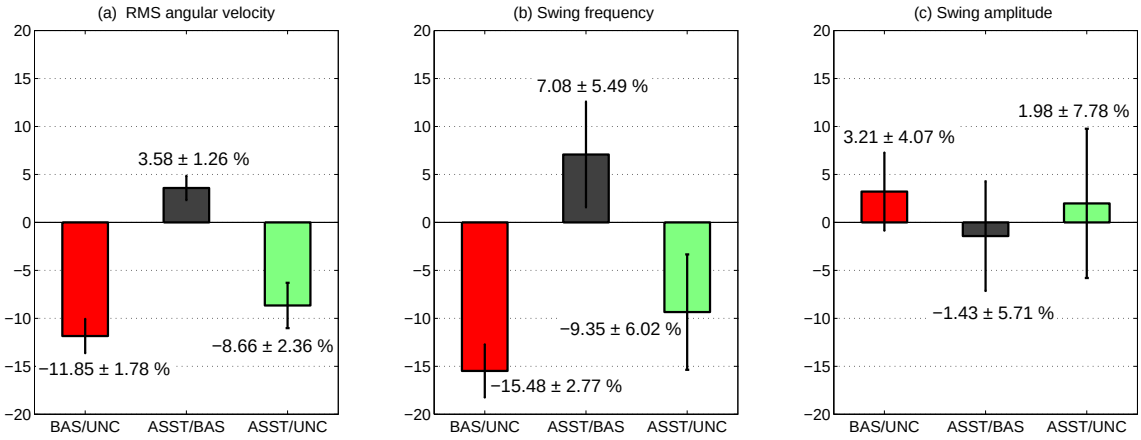

Figure 10: Transient phase: percentage variations (mean ± s.e.m.) among the different experimental conditions for (a) mean RMS angular velocity ($\Omega_{h,tr}$), (b) mean swing frequency ($f_{c,tr}$) and (c) mean swing amplitude ($A_{c,tr}$).

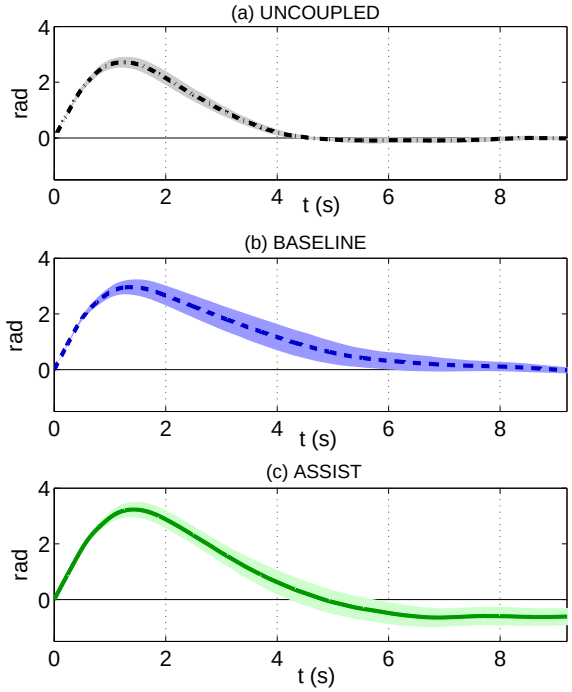

Figure 11: Averaged time histories of the position error $e_x(t)$, for the different experimental conditions: (a) UNCOUPLED, (b) BASELINE, (c) ASSIST. Plotted data are mean (lines) $\pm$ s.e.m. (shaded regions) of $e_x(t)$. The theoretical mean times for zero position error (zero-crossings of the horizontal axis) are also shown.

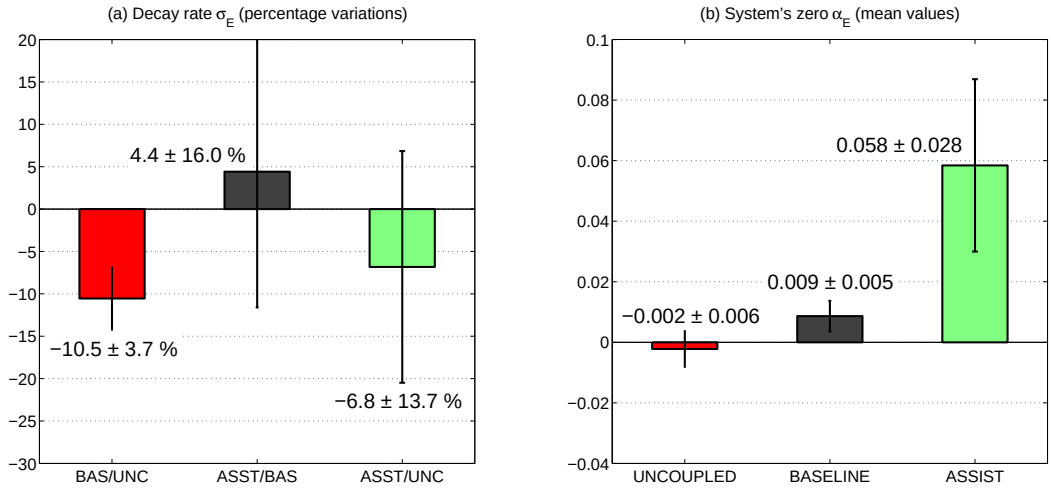

Figure 12: Position-error response modeled as a second-order system. (a) Percentage variations of the decay rate of the position error (σ_E) among the different experimental conditions: BASELINE vs. UNCOUPLED ($\bar{R}(\bar{\sigma_E})^{U,B}$), ASSIST vs. BASELINE ($\bar{R}(\bar{\sigma_E})^{B,A}$), and ASSIST vs. UNCOUPLED ($\bar{R}(\bar{\sigma_E})^{U,A}$). (b) Mean ± s.e.m. of the second-order system's zero (α_E) for each experimental condition.

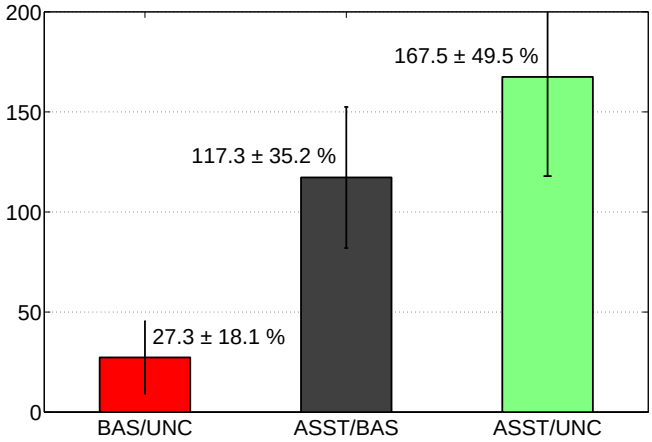

Figure 13: Percentage variations (mean ± s.e.m.) for the RMS position error during the steady-state phase, among the different experimental conditions: BASELINE vs. UNCOUPLED, ASSIST vs. BASELINE, and ASSIST vs. UNCOUPLED .

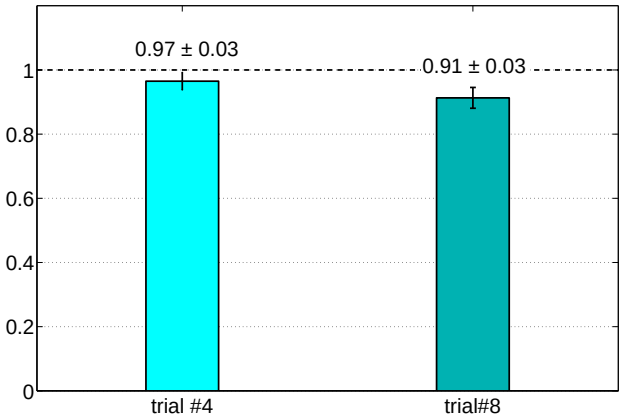

Figure 14: Mean ratios of RMS velocity for catch trials #4 and #8 in the ASSIST condition.